frontiers in Earth Science

ORIGINAL RESEARCH
published: 10 December 2020
doi: 10.3389/feart.2020.597469

Mineralogy of Nickel and Cobalt Minerals in Xiarihamu Nickel–Cobalt Deposit, East Kunlun Orogen, China

Yixiao Han[1,2], *Yunhua Liu*[1]* *and Wenyuan Li*[2]

[1] School of Earth Sciences and Resources, Chang'an University, Xi'an, China, [2] Key Laboratory for the Study of Focused Magmatism and Giant Ore Deposits, Ministry of Natural Resources, Xi'an Center of China Geological Survey, Xi'an, China

Located in the East Kunlun Orogen, China, the Xiarihamu magmatic nickel–cobalt sulfide deposit is the country's second largest deposit of this type. It was formed in special early Paleozoic with low copper grade (0.14 wt%) compared with other deposits of the same type. The mineralogy of nickel and cobalt minerals, which are direct carriers of these elements, can clearly reflect their behavior in the process of mineralization; however, such information for this deposit remains unreported. In the present study, we use an electron microscope and electron probe microanalyzer to delineate and analyze many nickel and cobalt minerals such as maucherite, nickeline, cobaltite, violarite, gersdorffite, parkerite, and arsenohauchecornite in various rocks and ores. With the increase in crustal material contamination, it can reach arsenide saturation locally in sulfide melt, then a separate Ni-rich arsenide (bismuth) melt exsolves somewhere. This melt will crystallize into nickeline, parkerite, arsenohauchecornite, and maucherite first. Second, most of nickel and cobalt tend to enter cobaltite and pentlandite phases, rather than existing in chalcopyrite and pyrrhotite phases as isomorphism during sufficient fractional crystallization of sulfide melt, which gathered nickel and cobalt elements widely. Also, more than one magma might result in the superposition of ore-forming elements. Later, the ore-forming elements redistribute limitedly through a hydrothermal process. The metallogenic mechanism model of nickel and cobalt established in the present study not only explains the process of nickel–cobalt mineralization in Xiarihamu but also can be applied to similar deposits and has a wide universal replicability.

Keywords: morphology, mineralogy, nickel–cobalt minerals, Xiarihamu, chemical compositions, mineralization model

OPEN ACCESS

Edited by:
Xiaohua Deng,
Beijing Institute of Geology for Mineral Resources, China

Reviewed by:
Yun Zhao,
China University of Geosciences, China
Shenghong Yang,
University of Oulu, Finland

***Correspondence:**
Yunhua Liu
Zyyhliu@chd.edu.cn

Specialty section:
This article was submitted to Petrology, a section of the journal Frontiers in Earth Science

Received: *21 August 2020*
Accepted: *26 October 2020*
Published: *10 December 2020*

Citation:
Han Y, Liu Y and Li W (2020) Mineralogy of Nickel and Cobalt Minerals in Xiarihamu Nickel–Cobalt Deposit, East Kunlun Orogen, China. Front. Earth Sci. 8:597469. doi: 10.3389/feart.2020.597469

INTRODUCTION

The strategic nickel and cobalt mineral resources in China play important roles in both civil and military fields. Although there are abundant magmatic sulfide deposits in China, they are mainly rich in copper and nickel, which are similar to large–superlarge magmatic sulfide deposits in the world. Cobalt occurs mostly as an accessory element and has not been the focus of significant attention (Zhao et al., 2019). This omission has caused a lack of systematic research in nickel–cobalt metallogenesis, which is inadequate considering the increased demand of these elements. The discovery of the Xiarihamu magmatic nickel–cobalt sulfide deposit, as the second largest nickel deposit in China, gives us an excellent opportunity to study occurrence states, genetic types, and metallogenesis of nickel and cobalt in minerals.

Globally, magmatic Ni–Cu–(PGE) sulfide deposits has occurred in a large range of periods, such as Archean, Paleoproterozoic, Mesoproterozoic, Neoproterozoic, and Paleozoic. But they have occurred mainly in early Neoproterozoic (1,000–800 Ma) and late Paleozoic (295–250 Ma) in China (Lü et al., 2007). Especially, the Xiarihamu magmatic nickel–cobalt sulfide deposit has special early Paleozoic (406–423 Ma) metallogenic age (Li et al., 2015; Song et al., 2016; Qian et al., 2020), representing a new metallogenic epoch of magmatic sulfide in China. The proven nickel metal reserve of the Xiarihamu deposit amounts to 1.18 Mt, with a grade of 0.23–3.48% and averaging 0.65 wt%, and that of cobalt metal is 40,300 t, with a grade of 0.012–0.079% and averaging 0.028 wt% (No. 5 Geological and Mineral Survey Institute of Qinghai Province, 2014). It has low copper grade (0.14 wt%) and lacks platinum group elements (Du et al., 2014). These characteristics attract us to explore the special enrichment process of nickel and cobalt in metallogenic evolution.

Previous studies have reported its geological characteristics (Yi et al., 2015), geochemistry of ore-bearing rocks (Jiang et al., 2015; Zhang Z.W. et al., 2016), various isotopes (Tang et al., 2017; Wang et al., 2018), rock and metallogenic ages (Wang et al., 2013; Ao et al., 2014; Wang et al., 2014b), and tectonic setting (Jiang et al., 2015; Li et al., 2015). The major elements of chromite, olivine, and pyroxene; rare earth elements; trace elements; and isotopes of bulk rocks indicate that the parental magma originated from partial melting of the asthenospheric mantle that was modified by melts derived from the subduction slab and subsequently underwent multiple-epoch silicate fractional crystallization and liquation of sulfides and silicates (Wang et al., 2014; Feng et al., 2016; Zhang Z.B. et al., 2016; Du, 2018; Song et al., 2020). Regarding the distribution, morphology, and geochemistry of pentlandite, pyrrhotite, and chalcopyrite in ores revealed that nickel occurs mainly as sulfides, whereas cobalt is usually isomorphically substituted for Ni^{2+} in pentlandite and violarite (Wang et al., 2014a; Feng et al., 2016).

Although strong positive correlation among nickel, copper, and cobalt has been reported, high-grade nickel ores are often closely correlated with cobalt, rather than copper, ores. Moreover, as direct carriers of ore-forming elements, nickel and cobalt minerals can be easily enriched through magma evolution, hydrothermal process, and weathering (Zhao et al., 2019). Identification of various mineralization stages is helpful in understanding the mineralization processes of nickel and cobalt.

In this study, we delineate the petrographic and textural characteristics of host rocks and sulfides of the Xiarihamu nickel–cobalt sulfide deposit. Based on these characteristics, the distribution, morphology, chemical compositions, and evolution history of the nickel and cobalt minerals are examined in detail to study the original ore-forming processes. The results reveal the enrichment mechanism of nickel and cobalt in the deposit and provide a strong clue to indicate the direction of prospecting high-grade ores in the future.

GEOLOGY OF THE XIARIHAMU DEPOSIT

The Xiarihamu mafic–ultramafic complexes are situated in the northern east/west-trending East Kunlun Orogen at the southern margin of the Qaidam Block, as a part of the Tarim Block in geological history (Li, 2018; Li et al., 2020) (**Figure 1A**). Five mafic–ultramafic complexes labeled I, II, III, IV, and V have been discovered in the Xiarihamu area (**Figure 1B**). The complexes were in the form of the lopolith that intruded metamorphic Jinshuikou group strata, which is composed of biotite granite gneiss, quartz schist, plagioclase amphibolite, marble, and Neoproterozoic granitic gneiss. And, they have a small exposed area presently. The faults are highly developed in this area in the east–west, northwest, and northeast directions. Diorite, syenogranite, and monzonite of various ages are also present.

The Xiarihamu magmatic nickel–cobalt sulfide deposit is hosted within the Xiarihamu I complex, which is located in the northern part of the central mining area. The Xiarihamu I mafic–ultramafic complex is irregularly shaped with an approximate length, width, and area of 1,600 m, 900 m, and 1.33 km^2, respectively, and a northeast–east strike of approximately 60°. The altitude of the complex is high in the east and low in the west. The middle and eastern parts of the Xiarihamu I complex are exposed at the surface, whereas the western part is concealed beneath the Jinshuikou group. The exposed complex is composed of dunite, pyroxenite, harzburgite, wehrlite, gabbronorite, and gabbro as well as sporadic oxidized ore (**Figure 1C**). The ore bodies, which occur in the peridotite and pyroxenite facies as well as part of the gabbro facies, are generally about 100–700 m long and 1.5–80 m thick and are mostly thick-layered and lenticular with a few funnel-shaped and irregular forms.

PETROLOGY OF INTRUSIONS

The No.15 exploration line is located in the western part of the mining area (**Figure 1**). The rocks have the integral lithofacies type of mafic–ultramafic rocks: dunite, harzburgite, wehrlite, pyroxenite, and gabbro (**Figure 2**). The ores are completely buried underground and show good mineralization. The characteristics of the mafic–ultramafic rocks vary among drill cores, as indicated by the lithofacies distribution and ore bodies observed in a cross section of this exploration line. Generally, compared with the rocks occurring in the south, the mafic–ultramafic rocks in the north have relatively simple lithology, deep buried, and low thickness, with local thickness of only 50 m, which is rich in high-grade ores (Ni > 1 wt%; Co > 0.03 wt%; Cu > 0.4 wt%).

More interestingly, a strong correlation is present between the grades of nickel and cobalt, rather than between those of nickel and copper. That is, a higher nickel grade corresponds with a richer cobalt grade (nickel > 1 wt%; cobalt > 0.03 wt%; **Figure 2**), which is also found in other exploration lines in this deposit (No. 5 Geological and Mineral Survey Institute of Qinghai Province, 2015). This phenomenon also occurs in

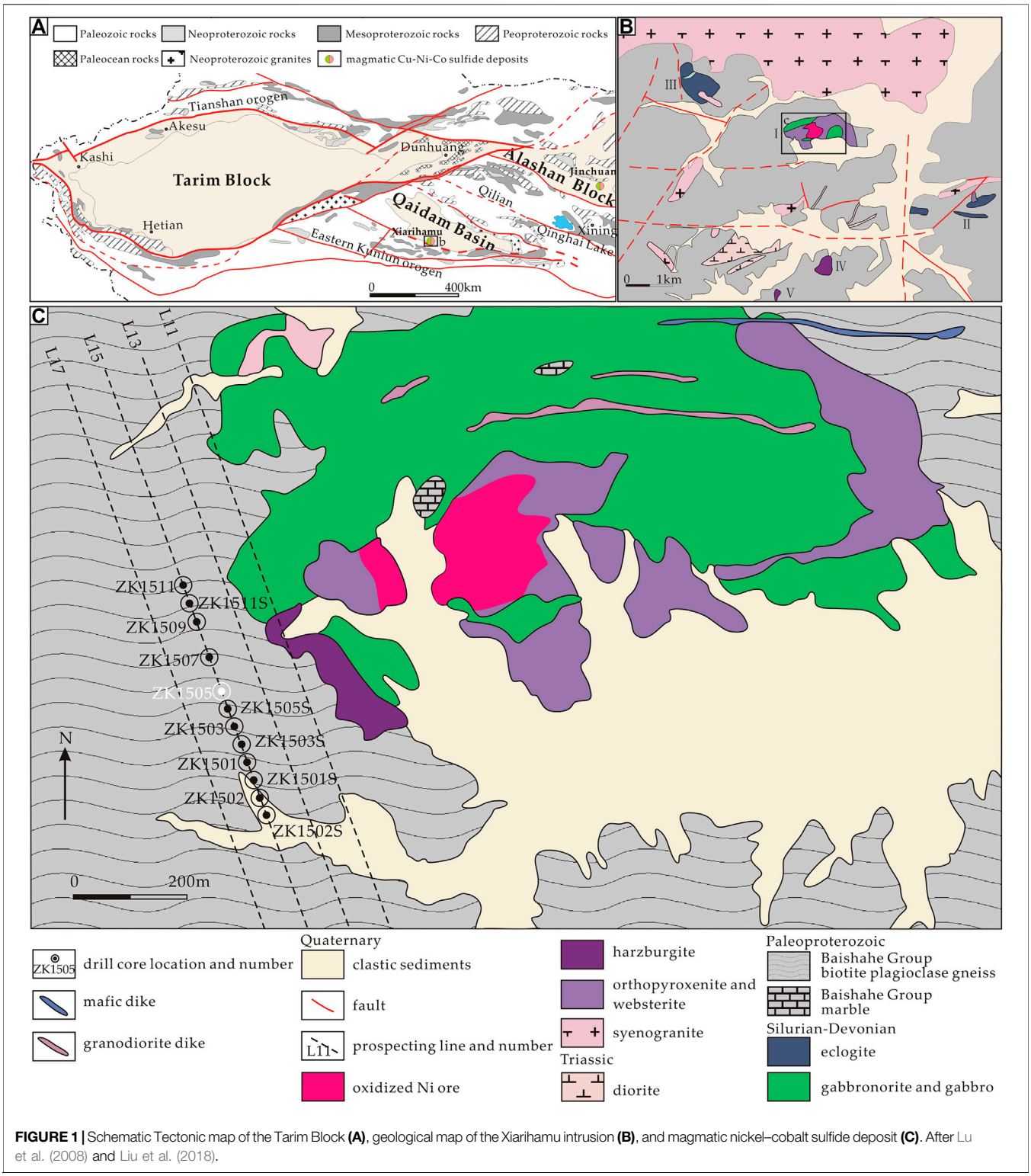

FIGURE 1 | Schematic Tectonic map of the Tarim Block **(A)**, geological map of the Xiarihamu intrusion **(B)**, and magmatic nickel–cobalt sulfide deposit **(C)**. After Lu et al. (2008) and Liu et al. (2018).

large copper–nickel–cobalt sulfide deposits such as Jinchuan deposit (Cao et al., 2010). To study the behavior of nickel and cobalt in the ore-forming processes, a ZK1505 drill hole was selected as the object of this research owing to its different lithofacies and ore-forming types as well as the strong correlation of cobalt and nickel grades.

Approximately 300-m-thick granitic gneiss of the Jinshuikou group is located in the upper part of ZK1505 drill core, and the

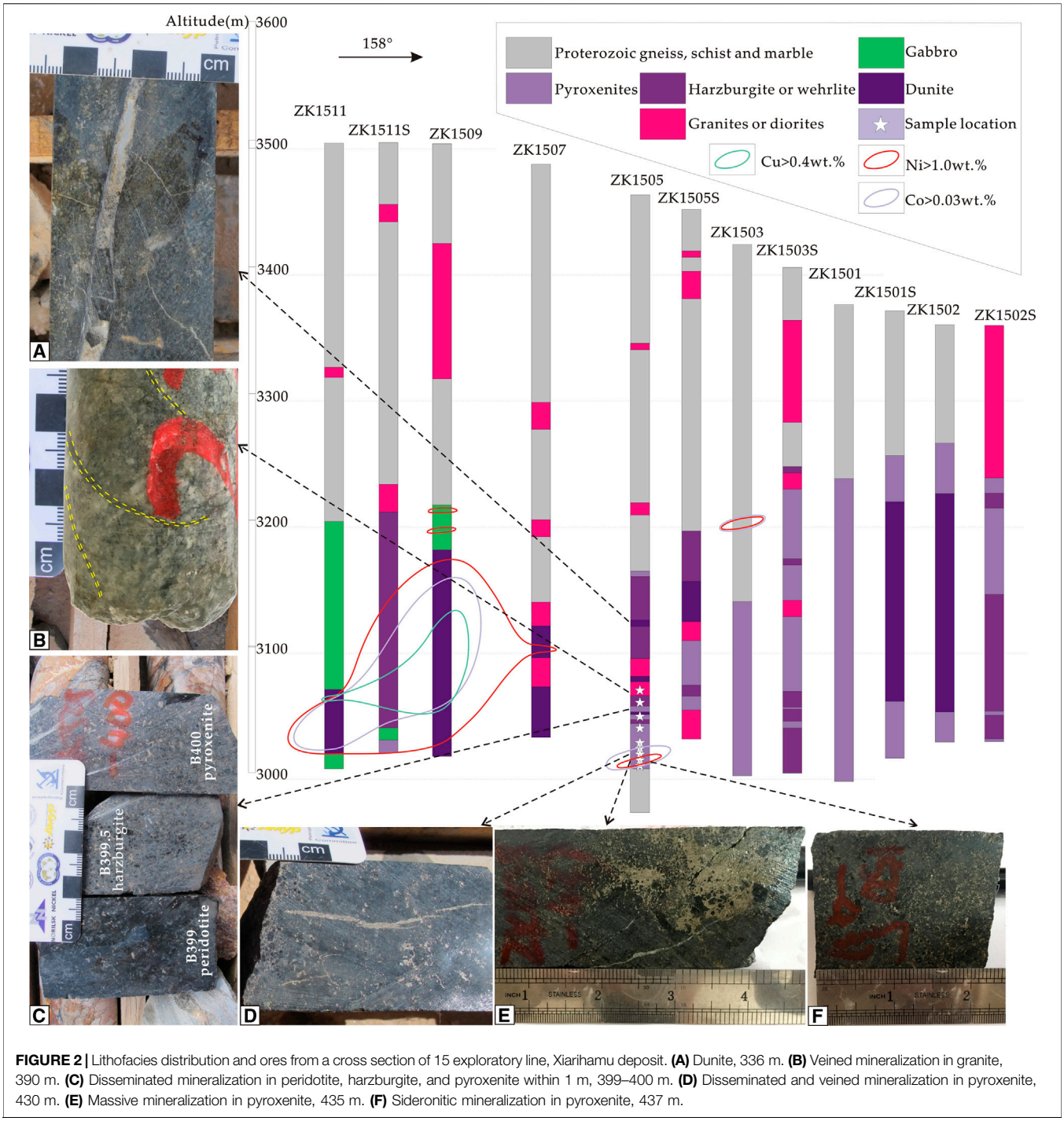

FIGURE 2 | Lithofacies distribution and ores from a cross section of 15 exploratory line, Xiarihamu deposit. **(A)** Dunite, 336 m. **(B)** Veined mineralization in granite, 390 m. **(C)** Disseminated mineralization in peridotite, harzburgite, and pyroxenite within 1 m, 399–400 m. **(D)** Disseminated and veined mineralization in pyroxenite, 430 m. **(E)** Massive mineralization in pyroxenite, 435 m. **(F)** Sideronitic mineralization in pyroxenite, 437 m.

mafic–ultramafic complex occurs mainly in the lower part, with some scattered granites in the drill core locally. In general, the distribution of mafic–ultramafic rocks and mineralization shows obvious trend. The upper part is composed of peridotite facies including dunite (**Figure 2A**), harzburgite, and wehrlite (**Figure 3A**), and the lower part is composed of pyroxenite facies including orthopyroxenite (**Figure 3B**) and websterite (**Figure 3C**). The mineralization types change gradually from top to bottom. At 300–400 m, there are mainly spotted, veined (**Figures 2B,D**), and disseminated (**Figure 2C**) mineralization, while massive (**Figure 2E**) and sideronitic mineralization (**Figure 2F**) occurs at 400–448 m. A gradual transition occurs between different rock types of a single lithofacies, and structural fracture zones or vein rocks often appear at the point of lithofacies change. In particular, veinlet mineralized granite (**Figure 2A**) occurs at 370–390 m,

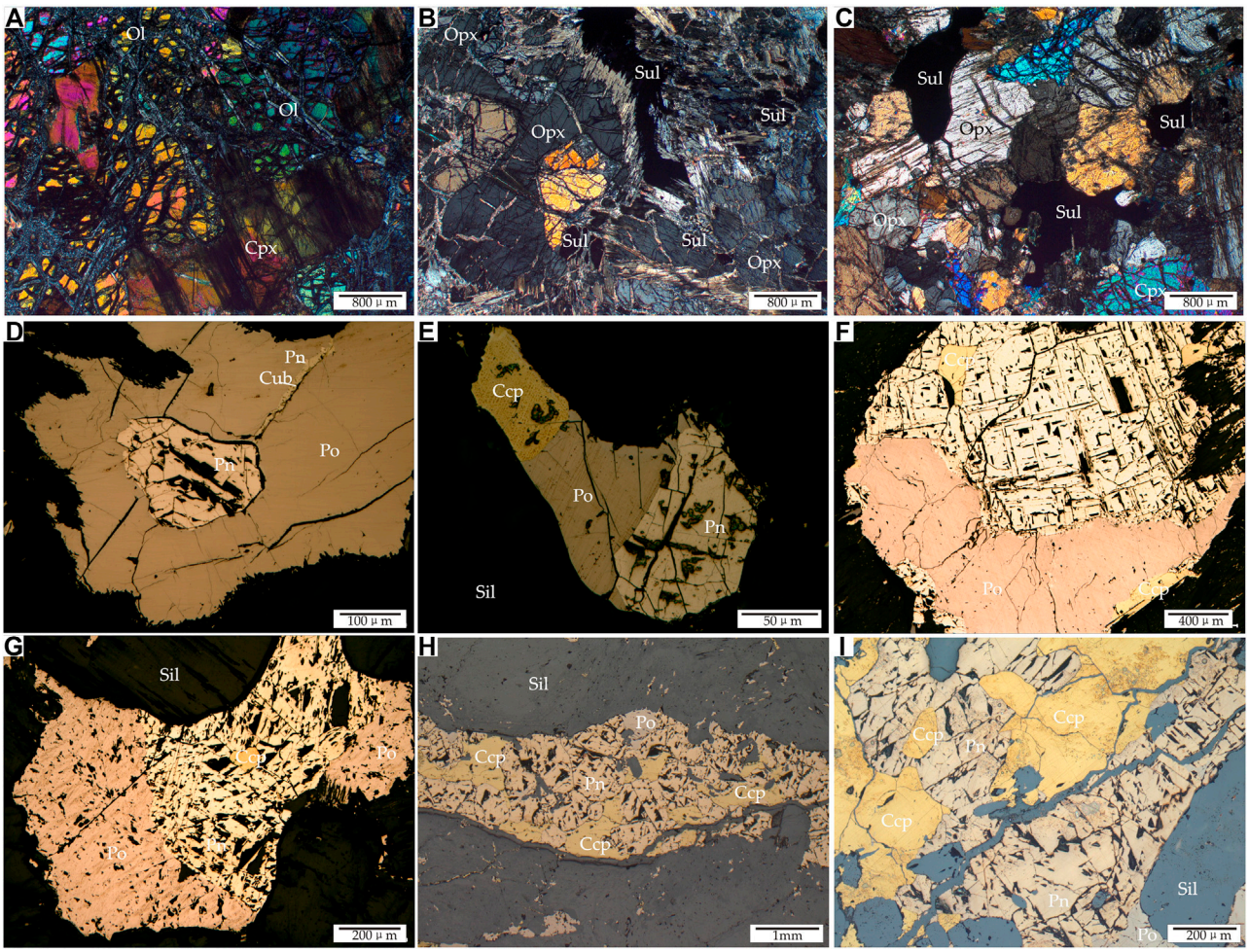

FIGURE 3 | Photomicrographs of sampling locations in main rock types (transmitted-light images) and sulfides (reflected-light images). **(A)** Wehrlite, 399.5 m. **(B,C)** Disseminated mineralization in orthopyroxenite and websterite, 400 and 427 m. **(D)** Po, filled with Cub vein in crack, encased Pn in pyroxenite, 406 m. **(E)** Ccp, Po, and Pn with straight borders in pyroxenite, 406 m. **(F,G)** Pn encased Ccp and contact with Po, in coarse disseminated mineralized pyroxenite, 418 and 427 m. **(H)** An increased quantity of Ccp in veined mineralized pyroxenite, 430 m. **(I)** More Ccp in massive mineralized pyroxenite, 442 m. Cpx, clinopyroxene; Ol, olivine; Opx, orthopyroxenite; Pn, pentlandite; Po, pyrrhotite; Ccp, chalcopyrite; Cub, cubanite; Sul, sulfide; Sil, silicate minerals.

where the lithofacies change. Within 1 m, at about 400 m, peridotite, harzburgite, and pyroxenite show transitional changes (**Figures 2C, 3A,B**). Below 400 m, the rock is essentially pyroxenite.

Pyrrhotite, pentlandite, and chalcopyrite are the main sulfides in the ores. Among them, pyrrhotite is the most abundant and chalcopyrite is the least. Pyrrhotite usually encloses pentlandite (**Figure 3D**) or occurs in a micrometer scale at the contact between chalcopyrite and pentlandite (**Figures 3E,F**). The chalcopyrite is in contact with pyrrhotite or enclosed by pentlandite (**Figures 3F,G**) in disseminated mineralization, and it coexists with pyrrhotite and pentlandite in veined and massive mineralization (**Figures 3H,I**). In addition, cubanite is observed in pyrrhotite cracks with pentlandite flames (**Figure 3D**).

EXPERIMENTAL METHODS

Although both nickel and cobalt minerals are visible in the 11, 13, 15, and 17 exploration lines, drill core ZK1505 includes different representative lithofacies and mineralization types (**Figure 2**). Therefore, it is considered as a suitable research object for studying the occurrence states and evolution behaviors of nickel and cobalt. For this study, 20 samples were collected from drill core ZK1505 in the central part of the ultramafic zone (**Figure 1C**). We conducted backscattering image observation, mineral chemical composition analysis, and element surface scanning analysis of ore minerals, particularly nickel and cobalt minerals and their associated minerals, using a JEOL JXA-8230 electron probe microanalyzer (EPMA) at Xi'an Center of China Geological Survey, Ministry of Natural

Resources. The analytical conditions for component analysis were 20 kV, 20 nA beam current, 1 μm beam size, 10 s peak-counting time, and 5 s upper and lower background counting time. In addition, the ZAF (atomic number, absorption, and fluorescence) correction method was used. The mineral standards of gallium arsenide (As 243), selenium (Se 97), chromium (Cr 145), pyrite (Fe 139, S 41), copper (Co 132), nickel (Ni 140), chalcopyrite (Cu 187), sphalerite (Zn 211), bismuth (Bi 231), cadmium (Cd 89), tellurium (Te 99), and stibnite (Sb 112) were used for calibration. The analytical conditions for element surface scanning were 20 kV, 100 nA, 0.3 μm step size, and 100 ms dwell time.

RESULTS

Distribution and Morphology of Nickel–Cobalt Minerals

The main ore minerals in the mining area are pyrrhotite, pentlandite, and chalcopyrite. Some nickel–cobalt minerals occur as accessory phases, as represented by nickel–arsenide, including maucherite ($Ni_{11}As_8$) and nickeline (NiAs), and sulpharsenides of nickel and cobalt such as gersdorffite (NiAsS) and cobaltite (CoAsS). In addition, nickel can also form minerals with some complex anions containing bismuth, arsenic, and sulfur. Parkerite ($Ni_3Bi_2S_2$) and arsenohauchecornite ($Ni_{18}Bi_3AsS_{16}$), which have been described in other superlarge copper–nickel deposits such as Sudbury (Michener and Peacock, 1943; Springer, 1989) and Noril'sk (Ponomarenko et al., 1987; Spiridonov et al., 2008), have not been described in magmatic copper–nickel sulfides in China. However, they are reported for the first time in the present study. Here, we delineate the microstructural characteristics of these minerals according to the different mineralization types, as shown in the backscattered electron images in **Figure 4**.

In the spotted mineralized peridotite above 399 m, there are pyrrhotite, pentlandite, and chalcopyrite locally and no other microscopically visible other nickel–cobalt minerals (except for pentlandite) appear. Below the depth of 399 m, xenomorphic maucherites (10 × 10–100 × 150 μm) are encased in pentlandite and pyrrhotite in the disseminated mineralized pyroxenite (**Figures 4A,B**). Euhedral nickelines and parkerites, with sizes of 10 × 20–30 × 80 μm, are encased in pentlandite and pyrrhotite (**Figures 4C,D**). The ores have sideronitic texture—massive texture at the bottom of the drill core at about 435–446 m. Euhedral–subhedral granular cobaltites, with sizes of 20 × 40–80 × 100 μm, always occur in the pyrrhotite margin and in contact with other sulfides or oxides in pyrrhotite–magnetite (**Figure 4E**), pyrrhotite–pentlandite–chalcopyrite (**Figure 4F**), pyrrhotite–pentlandite (**Figures 4G,H**), and pyrrhotite–chalcopyrite assemblages (**Figure 4I**). Several maucherites are dispersed in silicate minerals near the sulfides in this area (**Figure 4E**). They usually contain numerous inclusions of parkerite and arsenohauchecornite and display skeletal crystals (**Figures 4G–I**). Parkerites occur as 30 × 30 μm xenomorphic granular inclusions (**Figure 4I**) and scattered microparticles (**Figure 4F**) in the center of cobaltites in both primary pyrrhotite–pentlandite–chalcopyrite and pyrrhotite–pentlandite assemblages. Arsenohauchecornites, like some parkerites, occur as scattered microparticles in cobaltites in a primary pyrrhotite–pentlandite assemblage (**Figure 4G**).

Numerous veinlets (1–3 mm) are developed in the granites at 370–390 m (**Figure 2B**). Pyrrhotite–chalcopyrite–violarite veins are identified at 390 m, with maucherite, nickeline, and gersdorffite. The violarite, a less common iron–nickel sulfide, exhibits typical shrinkage characteristics of an exsolution product, which is dense at the core and clean at the edges (**Figure 4J**). Gersdorffite replaced pyrrhotite or chalcopyrite and displays a tight cluster now. A hackly erosion boundary was formed along fractures, and a few irregular metasomatic relict texture pyrrhotites and chalcopyrites occur inside during the metasomatism (**Figure 4K**). The enlarged image clearly shows the metasomatic structure of gersdorffite (**Figure 4L**). Granular nickelines are encased in pyrrhotite and violarite. Numerous xenomorphic granular maucherites developed in the cracks of pyrrhotite at the remote end of the metasomatic veined gersdorffite (**Figure 4K**), whereas others are nickelines with no metasomatic alteration.

Chemical Compositions of Nickel–Cobalt Minerals

The major and trace elements of the nickel and cobalt minerals are shown in **Table 1**. According to the above observations and EPMA data, the characteristics of the maucherites are different between the disseminated and vein mineralization types. The scattered xenomorphic granular maucherites in disseminated mineralization contain 45.52–46.80 wt% arsenic, 49.16–52.20 wt% nickel, and small amounts of iron and copper. In particular, cobalt replaced nickel by 0.25–0.33 wt%. In contrast, the maucherites contain 46.14–46.89 wt% arsenic and 51.13–52.27 wt% nickel with little fluctuation and substantially no cobalt in the veined mineralization. The major element (nickel, copper, cobalt, arsenic, and sulfur) maps of veined mineralization (**Figure 5**) clearly show that the maucherites experienced metasomatism together with pyrrhotite and chalcopyrite and are enclosed in a cobalt-bearing gersdorffite cluster.

The nickelines are composed of 4.26–44.48 wt% nickel, 53.3–54.53 wt% arsenic, and minute quantities of iron and copper. Tellurium replaced up to 1.16 wt% of arsenic.

The cobaltites contain 17.59–27.17 wt% cobalt, 5.84–13.01 wt% nickel, 45.58–43.04 wt% arsenic, 19.33–20.10 wt% sulfur, 3.41–5.24 wt% iron, and a small amount of tellurium, all belonging to various cobaltite–nickel cobaltites. The contents of cobalt and nickel show obvious inverse correlation in **Figure 6A**, which might be attributed to the form of cobaltite–gersdorffite solid solution or the varying degrees of pyrrhotite metasomatism.

The parkerites are composed of 25.38–28.11 wt% nickel, 61.88–64.98 wt% bismuth, and 9.80–10.03 wt% sulfur. The arsenohauchecornites are composed of 24.86 wt% arsenic, 15.63 wt% iron, 17.30 wt% cobalt, 5.66 wt% nickel, 21.89 wt% sulfur, and 16.32 wt% bismuth. Compared with the ideal formula

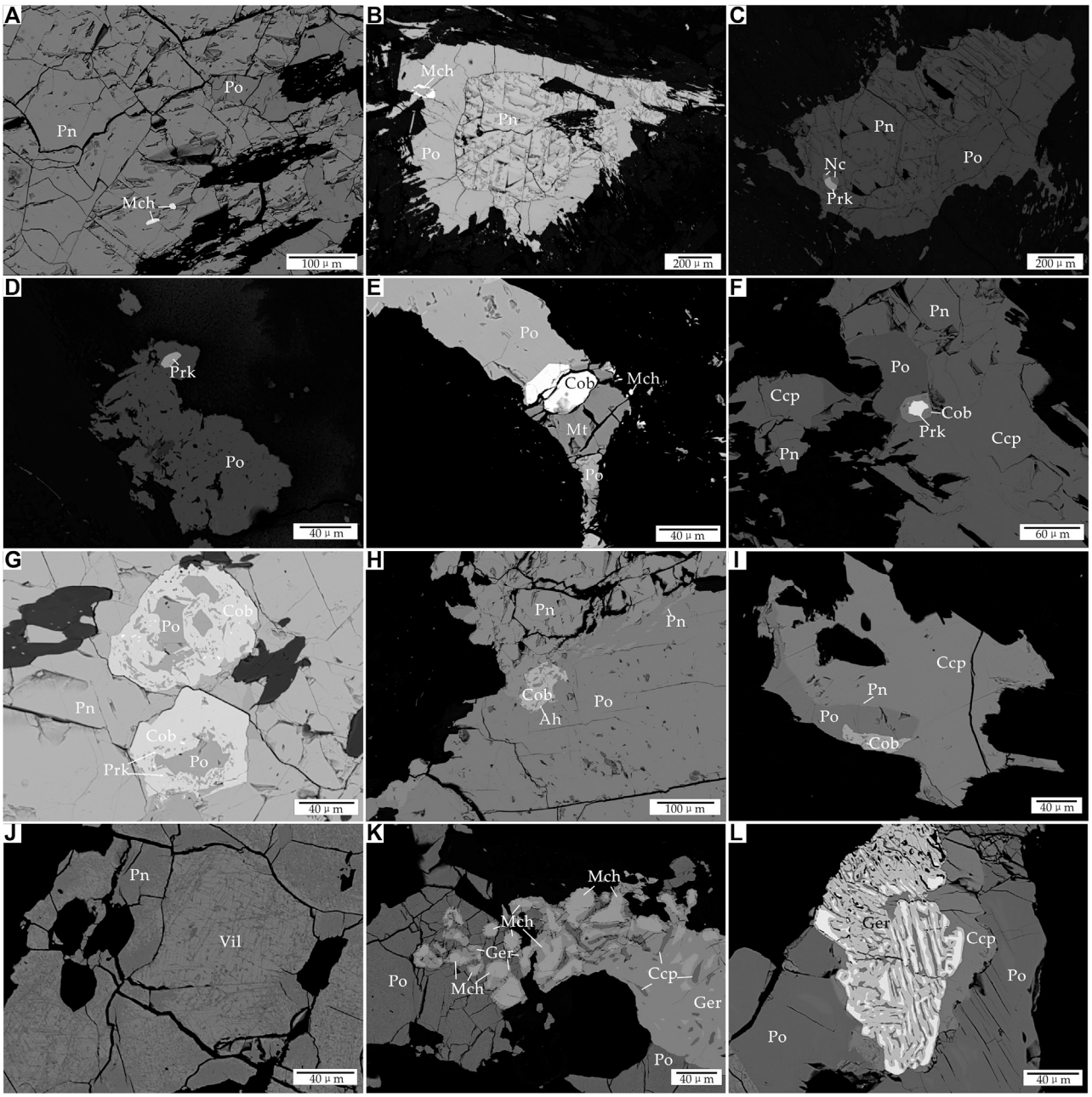

FIGURE 4 | Backscattered electron images of nickel–cobalt minerals and relevant minerals in ZK1505, Xiarihamu deposit. **(A,B)** Xenomorphic granular Mch are encased in Po and Pn, 399.5 m. **(C,D)** Euhedral Nc and Prk were encased in Pn and Po, 418 and 427 m. **(E)** Xenomorphic Mch dispersedly grows in silicate minerals near sulfide, 437 m. **(F)** Xenomorphic granular parkerite in the center of euhedral cobaltite, enclosed in Po, 444 m. **(G,H)** Skeletal crystals of cobaltites in Pn–Po assemblages, contained numerous inclusions of parkerite and arsenohauchecornite, 440 and 442 m. **(I)** Skeletal crystals of cobaltites in Po–Ccp assemblages, 442 m. **(J–L)** Violarite, subhedral-xenomorphic granular maucherites, grew in the crack of Po and metasomatic gersdorffite cluster in the veinlets of granites, 390 m. Po, pyrrhotite; Pn, pentlandite; Ccp, chalcopyrite; Nc, nickeline; Mch, maucherite; Cob, cobaltite; Ger, gersdorffite; Vil, violarite; Mt, magnetite; Prk, parkerite; Ah, arsenohauchecornite.

of arsenohauchecornite ($Ni_{18}Bi_3AsS_{16}$), the isomorphs of iron and cobalt substituted nickel in large quantities. The analyzed parkerite and arsenohauchecornite grains are too small to support physical characterization, which would result in inaccurate content data; however, the mineral identification is not affected.

The composition of the violarites is 24.08–26.15wt% iron, 35.22–36.59 wt% nickel, 35.64–38.03 wt% sulfur, and >1 wt% nickel/iron. However, this composition is different from that of its ideal composition, which is 18.52 wt% iron, 38.94 wt% nickel, and 42.54 wt% sulfur; in the former, the iron is higher, while the sulfur content is lower.

TABLE 1 | Electron probe microanalyzer data of nickel–cobalt minerals in ZK1505, Xiarihamu deposit.

	No.	As	Fe	Co	Ni	Cu	Zn	S	Bi	Cd	Se	Cr	Sb	Te	Total	Formula
Nickeline (NiAs)	B-418-12	54.53	0.66	0.10	44.31	—	—	0.23	—	0.01			—	0.97	100.80	$Ni_{1.03}As$
	B-418-13	54.12	0.40	0.12	44.26	—	—	0.24	—	0.01			—	0.18	99.32	$Ni_{1.04}As$
	B-390-13	53.94	0.43	0.05	44.19	0.26	—	0.19	—	0.01			0.17	0.35	99.58	$Ni_{1.05}As$
	B-390-10	53.37	0.44	0.02	44.45	0.04	—	0.23	—	—			0.14	0.30	98.98	$Ni_{1.06}As$
	B-390-24	54.51	0.58	0.05	43.97	0.41	—	0.21	—	—			0.11	1.16	100.99	$Ni_{1.03}As$
	B-390-27	54.53	0.38	—	44.48	0.20	—	0.20	—	—			0.20	0.20	100.20	$Ni_{1.04}As$
	B-440-27	53.97	3.23	0.14	43.26	0.05	—	0.25	—	0.01			—	0.98	101.89	$Ni_{1.02}As$
Cobaltite (CoAsS)	B437-1	44.86	3.99	23.76	8.37	—	—	19.76	—	—			—	0.09	100.82	$Co_{0.65}Fe_{0.12}Ni_{0.23}As_{0.97}S$
	B442-1	44.14	3.82	23.17	8.79	—	—	19.86	—	—			—	0.19	99.98	$Co_{0.63}Fe_{0.11}Ni_{0.24}As_{0.95}S$
	B442-2	44.41	3.88	24.16	8.77	—	—	19.96	—	—			—	0.06	101.24	$Co_{0.66}Fe_{0.11}Ni_{0.24}As_{0.95}S$
	B442-10	43.96	5.24	22.19	9.68	0.08	0.02	19.76	0.01	0.01			—	0.10	101.06	$Co_{0.61}Fe_{0.15}Ni_{0.27}As_{0.95}S$
	B442-14	44.61	3.94	27.17	5.84	—	—	19.74	—	0.02			—	0.08	101.40	$Co_{0.75}Fe_{0.11}Ni_{0.16}As_{0.97}S$
	B442-18	44.00	5.18	20.94	9.74	—	—	19.83	0.36	—			—	0.12	100.16	$Co_{0.57}Fe_{0.15}Ni_{0.27}As_{0.95}S$
	B442-20	44.63	3.81	24.17	8.27	—	—	20.10	—	—			—	0.16	101.14	$Co_{0.65}Fe_{0.11}Ni_{0.22}As_{0.95}S$
	B442-21	45.24	3.72	24.75	7.63	—	0.10	19.94	0.03	0.01			—	0.06	101.48	$Co_{0.68}Fe_{0.11}Ni_{0.21}As_{0.97}S$
	B442-23	44.51	3.41	23.02	9.69	—	—	19.71	0.02	—			—	0.21	100.58	$Co_{0.64}Fe_{0.10}Ni_{0.27}As_{0.97}S$
	B444-1	44.48	4.43	23.02	8.80	—	—	19.85	—	0.04			—	0.15	100.78	$Co_{0.63}Fe_{0.13}Ni_{0.24}As_{0.96}S$
	B444-2	43.61	4.44	25.28	7.05	—	0.02	20.07	—	—			—	0.04	100.51	$Co_{0.69}Fe_{0.13}Ni_{0.19}As_{0.93}S$
	B444-3	45.34	5.20	17.59	13.01	0.44	—	19.69	—	—			—	0.11	101.37	$Co_{0.49}Fe_{0.15}Ni_{0.36}As_{0.99}S$
	B446-1	45.16	5.02	22.38	8.47	—	—	19.77	0.03	—			—	0.18	101.00	$Co_{0.62}Fe_{0.15}Ni_{0.23}As_{0.98}S$
	B446-2	45.58	3.41	19.45	12.62	—	—	19.41	—	0.01			—	0.20	100.68	$Co_{0.55}Fe_{0.10}Ni_{0.36}As_{1.01}S$
Gersdorffite (NiAsS)	B-390-1	44.39	1.14	0.35	34.54	0.09		19.21		—	—	—	0.22	0.77	100.70	$Ni_{0.98}Fe_{0.03}Co_{0.01}As_{0.99}S$
	B-390-2	45.12	1.98	0.34	34.09	0.07		19.23		—	—	—	0.34	0.14	101.31	$Ni_{0.97}Fe_{0.06}Co_{0.01}AsS$
	B-390-3	43.96	1.22	0.23	33.37	0.02		19.27		0.03	—	—	0.57	0.08	98.73	$Ni_{0.95}Fe_{0.04}Co_{0.01}As_{0.98}S$
	B-390-4	44.98	2.60	0.26	33.18	0.41		19.10		—	—	—	0.34	0.10	100.96	$Ni_{0.95}Fe_{0.08}Co_{0.01}As_{1.01}S$
	B-390-5	43.89	1.86	0.67	32.94	0.15		18.87		—	—	—	0.31	0.79	99.48	$Ni_{0.95}Fe_{0.06}Co_{0.02}AsS$
	B-390-6	43.44	1.63	1.20	32.28	—		19.44		—	—	—	0.12	0.20	98.29	$Ni_{0.91}Fe_{0.05}Co_{0.03}As_{0.96}S$
	B-390-7	45.34	1.86	1.74	32.55	0.18		19.43		—	—	—	0.00	0.73	101.83	$Ni_{0.91}Fe_{0.05}Co_{0.05}AsS$
	B-390-8	44.22	2.83	2.78	30.70	0.01		19.65		—	—	—	0.13	0.16	100.48	$Ni_{0.85}Fe_{0.08}Co_{0.08}As_{0.96}S$
	B-390-9	44.82	2.51	2.34	30.98	0.10		19.46		—	—	—	0.25	0.86	101.30	$Ni_{0.87}Fe_{0.07}Co_{0.07}As_{0.99}S$
Violarite ($FeNi_2S_4$)	B390-10	0.06	24.08	0.13	35.22	0.07		38.03		—	—	0.01	—	0.29	97.89	$Fe_{1.45}Ni_{2.02}S_4$
	B390-11	0.12	25.21	0.05	35.67	0.01		36.78		—	0.03	—	—	0.73	98.60	$Fe_{1.57}Ni_{2.12}S_4$
	B390-12	—	26.15	0.06	35.83	0.03		35.64		—	—	—	—	0.81	98.51	$Fe_{1.69}Ni_{2.20}S_4$
	B-390-13	—	24.93	0.15	36.59	—		37.43		—	—	0.03	—	0.72	99.85	$Fe_{1.53}Ni_{2.14}S_4$
Maucherite ($Ni_{11}As_8$)	B-399.5-10	46.80	0.91	0.25	52.20	—	—	0.12	—	0.04			—	0.34	100.67	$Ni_{11.39}As_8$
	B-399.5-13	45.52	2.28	0.33	51.00	0.07	—	0.24	—	—			—	1.14	100.58	$Ni_{11.44}As_8$
	B-406-10	45.64	3.35	0.30	49.16	0.23	—	0.36	—	0.03			—	0.37	99.44	$Ni_{11}As_8$
	B-406-12	46.18	2.81	0.30	51.25	0.06	—	0.18	—	0.03			—	0.48	101.28	$Ni_{11.33}As_8$
	B-390-14	46.89	0.62	0.00	52.27	0.04		0.15		0.06	—	—	—	1.13	101.15	$Ni_{11.38}As_8$
	B-390-15	46.14	1.12	0.01	51.13	0.15		0.18		—	—	—	—	1.07	99.80	$Ni_{11.32}As_8$
	B-390-16	46.17	0.12	0.00	51.95	0.05		0.16		—	—	—	—	0.33	98.79	$Ni_{11.49}As_8$
	B-390-17	46.78	0.33	0.02	52.03	0.09		0.13		—	—	—	—	1.34	100.72	$Ni_{11.36}As_8$
Parkerite ($Ni_3Bi_2S_2$)	B-442-11	—	0.70	0.01	25.38	0.71		10.03	61.88		0.02	1.15	—	0.17	100.05	
	B-446-3	—	0.43	—	26.88	0.28		9.80	63.65		—	1.10	0.31	0.67	103.11	
	B-444-25	—	0.52	0.21	28.11	0.13		9.91	64.98		0.01	1.03	0.26	0.86	106.01	
	B-399.5-28	—	0.83	0.02	27.50	0.42		10.03	64.67		0.04	1.15	0.89	—	105.53	
Arsenohauchecornite ($Ni_{18}Bi_3AsS_{16}$)	B-440-24	24.86	15.63	17.30	5.66	—		21.89	16.32		—	—	—	0.01	101.67	

Notes: "—", below the detection limit; blanks, unanalyzed or not calculated.

The gersdorffite compositions are as follows: 0.225–2.782 wt% cobalt, 30.70–34.54 wt% nickel, 43.44–45.34 wt% arsenic, 18.87–19.65 wt% sulfur, 1.14–2.83 wt% iron, and trace amounts of tellurium, antimony, and copper. The nickel content ranges from 0.85 to 0.98 atoms per formula unit (apfu). As shown in **Figure 5B**, the contents of cobalt and nickel exhibit obvious inverse correlation. The abnormality of individual points might be related to the degree of metasomatism. In the major element (nickel, copper, cobalt, arsenic, and sulfur) maps shown in **Figure 6B**, the cobalt content of gersdorffites is not evenly distributed at the edges of nickeline and the central vein.

DISCUSSION

Due to the special cobalt and nickel mineralization in the Xiarihamu magmatic sulfide deposit, whether there exist a special enrichment and evolution mechanism of nickel and cobalt is particularly important. The previous study proposes hydrothermal genesis of cobaltites (Wang, 2014), which is inconsistent with our study. The extensive appearances of nickel and cobalt minerals including cobaltites are closely related to high-grade ores in the deposit. So, it is necessary to interpret the genesis clearly.

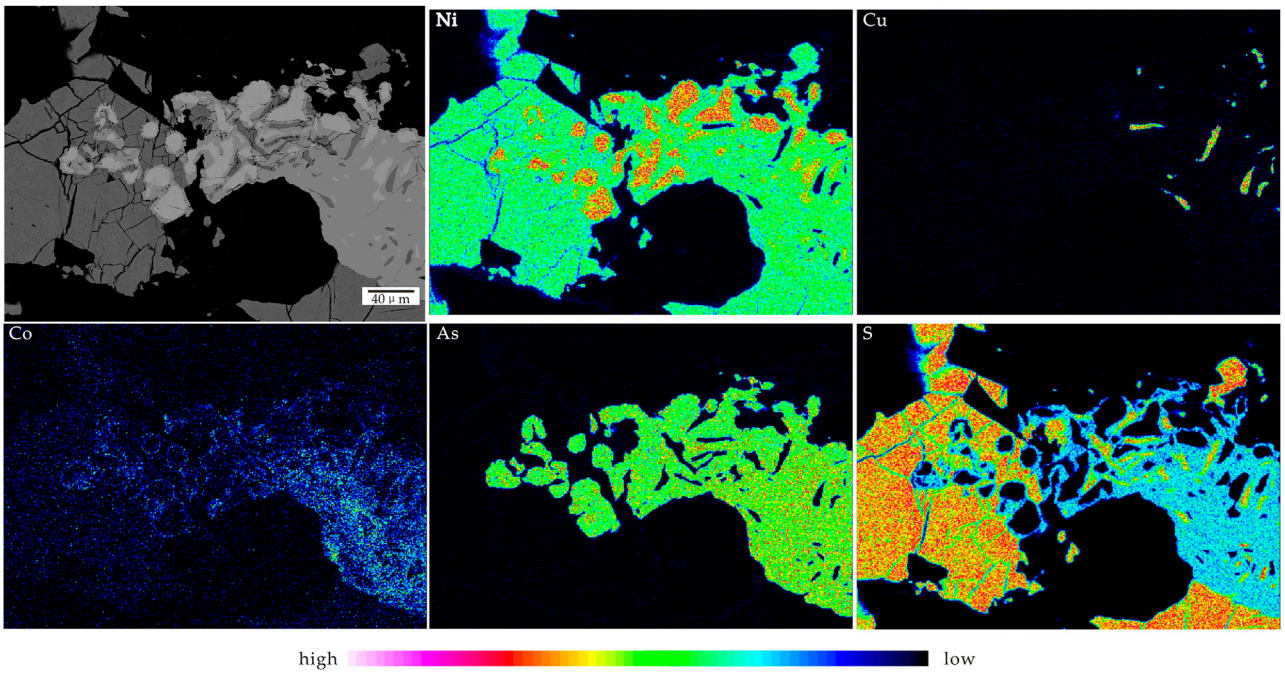

FIGURE 5 | Major element (Ni, Cu, Co, As, and S) maps of vein mineralization in ZK1505, Xiarihamu deposit.

Enrichment of Nickel and Cobalt

Previous studies indicated that when a natural sulfide melt reaches arsenide saturation (and probably many other chalcogens and metalloids in magmatic melts), a separate Ni–PGE-rich arsenide (bismuth) melt exsolves (Helmy et al., 2013). And, the affinities of the chalcophile metals for an immiscible arsenide melt follow the order Pt > Pd > Ni >> Fe ≈ Cu. This phenomenon conceivably occurs in nature (Fleet, 1973; Piña et al., 2014) and plays an important role in the mineralization of many cobalt deposits. Thus, if they reach arsenide (bismuth) saturation, we cannot simply explain the formation of such kind of minerals as forming at the late stage of sulfide melt fractionation because of the low partition coefficients between the monosulfide solid solution (MSS) and the melt (Helmy et al., 2010; Helmy et al., 2013; Liu and Brenan, 2015). Small subhedral-xenomorphic granular arsenic- or bismuth-bearing minerals (nickeline, parkerite, arsenohauchecornite, and maucherite) were enclosed in base metal sulfides in sideronitic massive ores rather than spot-disseminated ores in Xiarihamu. Hence, it reveals that sulfide saturation occurs in the magma during a large amount of crustal material contamination (Liu et al., 2018).

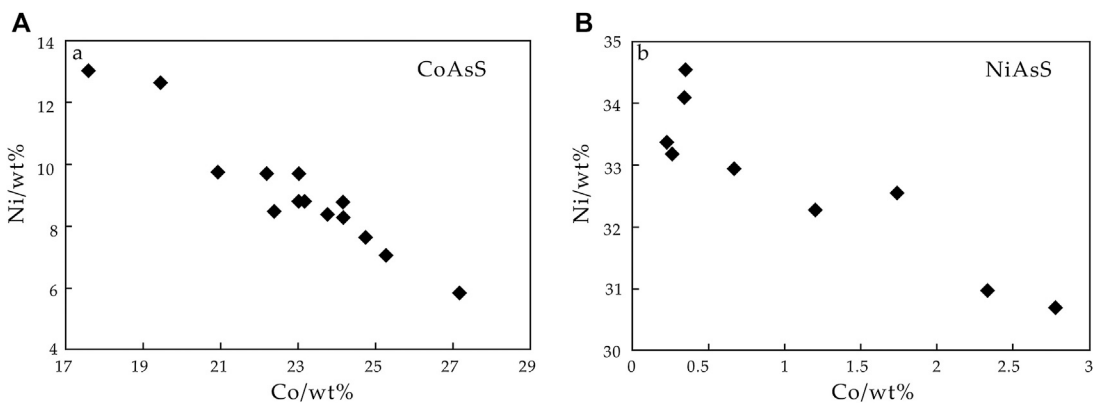

FIGURE 6 | Co–Ni (wt%) diagram of cobaltite **(A)** and gersdorffite **(B)**.

TABLE 2 | Grade of nickel and cobalt in ZK1505, Xiarihamu deposit.

	Depth/m	Ni/wt%	Co/wt%
H1	295–296.8	0.023	0.0014
H2	296.8–298	0.16	0.0079
H3	298–300	0.12	0.0072
H4	300–302	0.13	0.0083
H5	302–304	0.12	0.0084
H6	304–306	0.13	0.0093
H7	306–308	0.13	0.0078
H8	308–310	0.14	0.0092
H9	310–312	0.15	0.0099
H10	312–314	0.17	0.01
H11	314–316	0.16	0.0095
H12	316–318	0.16	0.01
H13	318–320	0.17	0.011
H14	320–322	0.17	0.01
H15	322–324	0.17	0.01
H16	324–326	0.18	0.011
H17	326–328	0.19	0.011
H18	328–329.83	0.25	0.012
H19	329.83–331	0.34	0.012
H20	331–333	0.26	0.012
H21	333–335	0.31	0.012
H22	335–337	0.32	0.012
H23	337–339	0.43	0.014
H24	339–341	0.28	0.011
H25	341–343	0.17	0.01
H26	343–345	0.1	0.0066
H27	345–347	0.067	0.003
H28	347–349	0.24	0.01
H29	349–351	0.17	0.0095
H30	351–353	0.18	0.011
H31	353–355	0.18	0.011
H32	355–357	0.21	0.012
H33	357–359	0.25	0.013
H34	359–360.56	0.22	0.011
H35	360.56–362	0.17	0.0088
H36	375–376.56	0.0056	0.0004
H37	376.56–378	0.39	0.013
H38	378–380	0.52	0.016
H39	380–381.18	0.16	0.0073
H40	381.18–383	0.022	0.0005
H41	389–390.84	0.19	0.0044
H42	390.84–392	0.64	0.012
H43	392–394	0.57	0.017
H44	394–396	0.39	0.014
H45	396–398	0.51	0.014
H46	398–400	0.58	0.016
H47	400–402	0.9	0.019
H48	402–404	0.87	0.018
H49	404–406	0.72	0.017
H50	406–408	0.82	0.019
H51	408–410	0.82	0.018
H52	410–412	0.72	0.019
H53	412–414	0.73	0.02
H54	414–416	0.57	0.015
H55	416–418	0.79	0.018
H56	418–420	0.76	0.019
H57	420–422	0.66	0.02
H58	422–424	0.39	0.016
H59	424–426	0.43	0.02
H60	426–428	0.5	0.023
H61	428–430	0.57	0.025
H62	430–432	0.73	0.03
H63	432–434	0.64	0.026
H64	434–436	0.66	0.027
H65	436–438	0.89	0.034
H66	438–440	0.68	0.027
H67	440–442	0.77	0.03
H68	442–444	1.25	0.044
H69	444–446	0.87	0.031
H70	446–447.14	1.13	0.038
H71	447.14–449	0.065	0.0024
H72	449–451	0.0075	0.0009

(Continued in next column)

(*Continued*) Grade of nickel and cobalt in ZK1505, Xiarihamu deposit.

With the increase in crustal material contamination, it can reach arsenide saturation locally in sulfide melt, then a separate Ni-rich arsenide (bismuth) melt exsolves somewhere. Arsenic, bismuth, and little sulfur could potentially combine with nickel and cobalt to form these Ni- and Co-bearing accessory minerals because of PGE depletion in magma during sulfide liquation. Also, previous studies have shown that maucherites, as very common accessory phases, often occur in magmatic environments of 600–830°C (Yund, 1961; Roseboom, 1962; Singleton and Nash, 1987; Shvedov and Barkov, 2017). We propose that it might represent the crystallization temperature of Ni-rich arsenide (bismuth) melt, after the crystallization of olivine and pyroxene. These minerals mostly occur in base metal sulfides and just a little in silicate minerals (**Figure 4E**) which reveals that they are easy to move forward in sulfide melt rather than separating out like olivine and pyroxene. Since the arsenide melt crystallizes first and then the sulfide melt crystallizes, base metal sulfides contain a large number of arsenic- or bismuth-bearing minerals.

It can be inferred that sulfide melts have sufficient fractional crystallization because the boundaries among pentlandite, pyrrhotite, chalcopyrite, and cobaltite are mostly straight. Nickel usually enters pentlandite phase. And, most of cobalt tends to enter cobaltite phase with arsenic and sulfur, rather than existing in chalcopyrite and pyrrhotite as isomorphs when temperature slowly decreases, which can gather cobalt to a great extent.

The crystallization of Ni-rich arsenide (bismuth) melt and sufficient crystallization of sulfide melt largely gathered nickel and cobalt in nickel–cobalt minerals instead of being scattered as isomorphs in extensive pyrrhotite or chalcopyrite; that is the special metallogenic process of the Xiarihamu deposit.

Nickel and Cobalt Behavior in the Magma System

Based on whole-rock nickel and cobalt contents of the deposit (No. 5 Geological and Mineral Survey Institute of Qinghai Province, 2014), the grades of nickel and cobalt in ZK1505 significantly increased below 400 m, up to 1.25 (wt%) and 0.045 (wt%), respectively (**Table 2**; **Figure 7**). As mentioned previously, the rock type changes from peridotite in the upper part to pyroxenite in the lower part at about 400 m, regardless of the depth of the upper surrounding rock, while the ore type

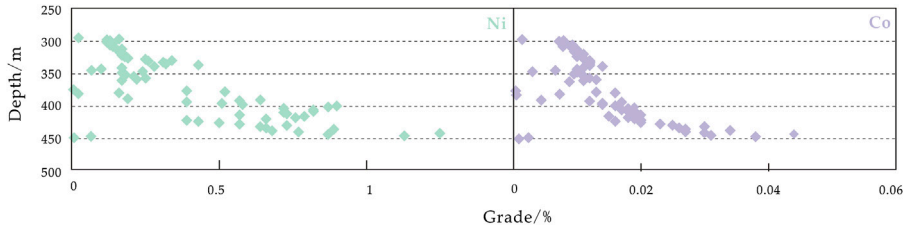

FIGURE 7 | Variation diagram of ZK1505 Ni and Co grades with depth in ZK1505, Xiarihamu deposit.

changes from spotted to sideronitic massive. More importantly, some cobalt and nickel minerals (nickeline, maucherite, and cobaltite) appear in large quantities below 400 m and are not present above that depth (only appearing pentlandite, pyrrhotite, and chalcopyrite), except for the vein at 390 m. From macroscopic to microcosmic observation, we consider that the position at which the nickel and cobalt grades are significantly increased are also the locations in which numerous nickel and cobalt minerals (nickeline, maucherite, and cobaltite) are developed. And in the low-grade ores, cobalt mainly exists in the form of isomorphism substitution of some nickel in pentlandites. Therefore, the formation of abundant nickel–cobalt minerals in the magmatic system greatly improves the ore grade.

When sulfide saturation occurs in the magma, nickel and cobaltite tend to enrich in sulfide melt due to high partition coefficient between sulfide and silicate melts (Crocket and Fleet, 1997; Li and Audétat, 2012). Cobaltite is a primary mineral. It is formed at the edge of pyrrhotite and other minerals and also contains pyrrhotite. It seems that it is formed by replacing pyrrhotite. But it shows euhedral or subhedral structure and has straight boundaries with other base metal sulfides, indicating symbiotic combination of them. In theory, when MSS and intermediate solid solutions (ISS) crystallized, the semimetal-rich melt remained liquid (Helmy et al., 2007). Thus, it can easily move to the edges of the cobalt- and nickel-rich MSS. Then, the semimetal-rich melt the remained liquid provides arsenic, and sulfide melt provides nickel, cobalt, and sulfur, which causes the combination to cobaltite during temperature reduction. Due to the large amount of pyrrhotites crystallized at this time, cobaltites experienced insufficient nucleation. It causes that cobaltites are enclosed in pyrrhotites and located at the boundaries between pyrrhotites and other minerals, and also some pyrrhotites are enclosed in cobaltites. Based on the FeAsS–CoAsS–NiAsS diagram (Klemm, 1965), the data almost plot in the 500–600°C isotherms, indicating 500–600°C formation temperature of cobaltites (**Figure 8**). Such textural relationships and formation temperature both indicate that cobaltites and base metal sulfides approximately formed at the same time. Most nickel, iron, sulfur, and little isomorphism cobalt form pentlandite, while most cobalt, some nickel, arsenic, and sulfur form cobaltite.

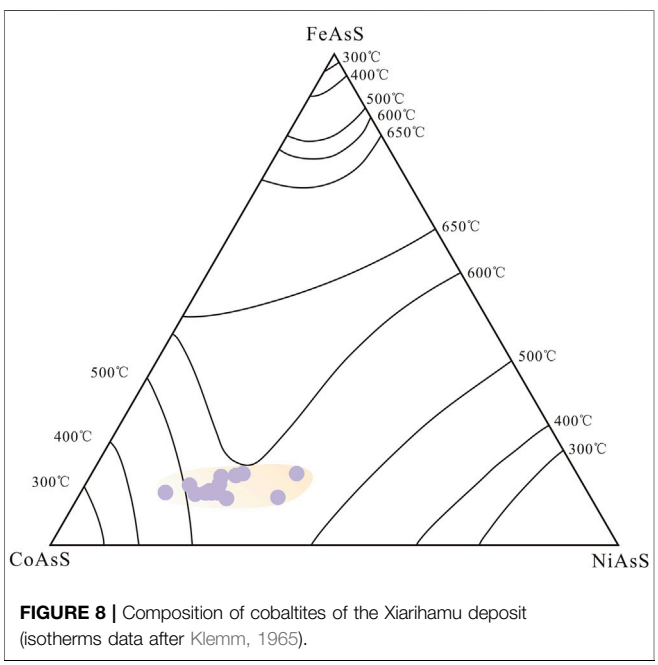

FIGURE 8 | Composition of cobaltites of the Xiarihamu deposit (isotherms data after Klemm, 1965).

In particular, pyrrhotite–chalcopyrite–pentlandite–violarite mineral assemblage occurs in veined mineralization at 390 m. Many researchers have concluded that violarite progressively replaces pentlandite as an outer rim of the coarse grains in the pentlandite as a result of hydrothermal alteration or weathering, as indicated by the fine-grained, porous, and finely cracked features (Craig, 1971; Tenailleau et al., 2006; Xia et al., 2009). However, the texture of the violarite in the present study (**Figure 3B**) is quite different, which is dense at the core and clean at the edges. Violarites are distributed along crystal face (111) of the early generation pentlandites, and it shows special shrinkage characteristics of an exsolution product. Violarites are formed by the decomposition of stable pentlandite solid solution in sulfide melt at lower temperature (Luo, 1994). In addition, the experiments revealed that violarites are stable below 461 ± 3°C and can form as a hypogene phase by primary direct crystallization or by secondary exsolution from an initially homogeneous MSS phase in the iron–nickel–sulfur system (Craig, 1971). The abnormally high iron content in the violarites indicates that its crystallization might not have been direct; rather, secondary exsolution from an initially homogeneous MSS phase might have occurred instead. Hence, it belongs to primary violarite here based on the above studies. The veined mineralization might be formed in lower temperature below 461 ± 3°C.

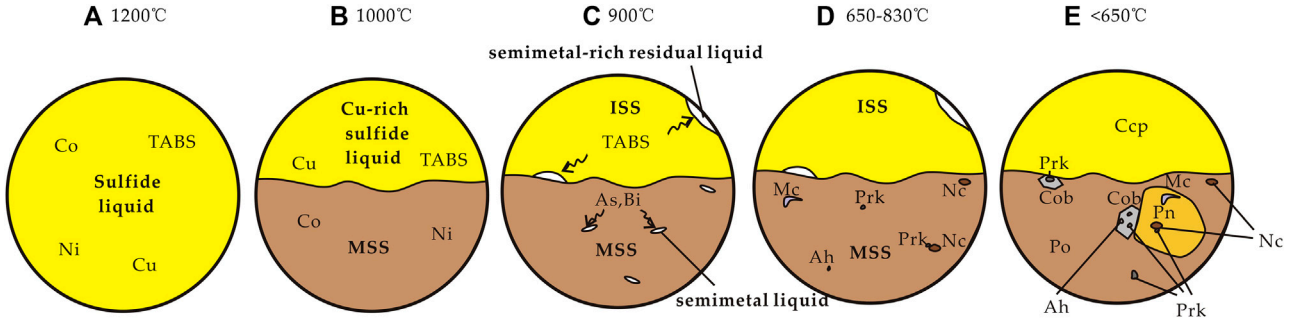

FIGURE 9 | Schematic model illustrating crystallization history of sulfide liquid in segregation-injection ores. MSS, monosulfide solid solution; ISS, intermediate solid solution; Ccp, chalcopyrite; Po, pyrrhotite; Pn, pentlandite; TABS, Te, As, Bi, Sb, and Sn; Cob, Ni–cobaltite; Prk, parkerite; Ah, arsenohauchecornite; Vil, violarite; Nc, nickeline; Mch, maucherite.

Moreover, maucherites also grew in the cracks of earlier pyrrhotites and were enclosed in the gersdorffites in veined mineralization. These high-temperature Co-poor maucherites (Yund, 1961; Roseboom, 1962; Singleton and Nash, 1987; Shvedov and Barkov, 2017) here are different with those Co-rich maucherites occurred during early magmatism in occurrence and composition characteristics. It implies another magma invaded this location prior to hydrothermal mineralization (in the next section), which might lead to changes in the early rock sequence at about 400 m (**Figure 2C**) and additional rapid nickel and cobalt mineralization.

Mineralization Model of Nickel and Cobalt

There are three different types of ore: *in situ* liquation (spot-disseminated ores), deep segregation-injection (sideronitic massive veined ores), and hydrothermal superposition (veined ore added secondary metasomatism) (Tang and Li, 1995). Among them, the segregation-injection ores are the most important type in the deposit. So the following nickel–cobalt evolution model is proposed, based on their textural relationships and geochemical behavior.

Figure 9 schematically shows the behavior of cobalt and nickel during arsenic and sulfide saturation from magmatic temperatures in segregation-injection ores. At magmatic temperatures of about 1,200°C, the sulfide liquid contained dissolved nickel, cobalt, copper, iron, tellurium, arsenic, bismuth, antimony, and tin (**Figure 9A**). Upon cooling to about 1,000°C, partial cobalt and nickel were concentrated in MSS, while tellurium, arsenic, bismuth, antimony, and tin partitioned into the copper-rich residual liquid after MSS crystallization (**Figure 9B**). Upon further cooling to about 900°C, ISS crystallized out of the residual liquid, and the semimetal-rich melt remained liquid (**Figure 9C**) (Helmy et al., 2007). At about 650–830°C, Ni-rich arsenide (bismuth) melt exsolved occasionally and formed parkerite, arsenohauchecornite, maucherite, and nickeline with nickel and cobalt because of arsenide saturation locally (**Figure 9D**). At low temperatures, when MSS and intermediate solid solutions (ISS) exsolved into pyrrhotite, pentlandite, and chalcopyrite below 650°C (Mansur et al., 2019), arsenic derived from the semimetal-rich residual liquid and combined with nickel, cobalt, and sulfur to form cobaltite (**Figure 9E**). They contained early parkerite, arsenohauchecornite, maucherite, and nickeline during crystallization. Then, the residual nickel formed in the pyrrhotite–chalcopyrite–pentlandite–violarite veins, which occur in structural weakness zones under a temperature of about 461°C.

Nickel and Cobalt Behavior in the Hydrothermal System

The primary vein mineralization was magmatic as mentioned above. But the pyrrhotite and chalcopyrite were not completely metasomatized by the gersdorffite cluster along the fracture in the granite and formed a hackly erosion boundary along fractures (**Figures 4K,L, 5K**), which might support their hydrothermal origin (Raič and Mogessie, 2015; Hazen et al., 2017; Moroni et al., 2017; Manuel et al., 2018; Stefan et al., 2018; Liang et al., 2019; Huang et al., 2020). During hydrothermal processes, nickel and cobalt in the silicate mineral lattice or earlier minerals were extracted or dissolved. In the process of migration to the structural weakness zones, the gersdorffite cluster redeposited and metasomatized the early minerals along the granite fractures. Although the hydrothermal source cannot be explained by the existing phenomena and data, its contribution to the deposit is extremely limited.

CONCLUSION

Almost all nickel–cobalt minerals are primary minerals, except gersdorffite. Only limited ore-forming elements redistribute during hydrothermalism. The crystallization of Ni-rich arsenide (bismuth) melt and sufficient crystallization of sulfide melt together constitute the special enrichment and evolution mechanism of nickel and cobalt in the Xiarihamu deposit.

DATA AVAILABILITY STATEMENT

The original contributions presented in the study are included in the article; further inquiries can be directed to the corresponding author.

AUTHOR CONTRIBUTIONS

YH: investigation, methodology, analysis, writing, and original draft preparation; YL and WL: writing, review, and editing; YH and YL: funding acquisition.

FUNDING

This work was jointly supported by the Fundamental Research Funds for the Central Universities, CHD (300102278711), the National Natural Science Foundation of China (211027180410), and the National Key R&D Program of China (2017YFC0601205).

ACKNOWLEDGMENTS

The authors thank the reviewers for providing critical comments and suggestions.

REFERENCES

Ao, C., Sun, F. Y., Li, B. L., Li, S. J., and Wang, G. (2014). Geochemistry, zircon U-Pb dating and geological significance of diorite porphyrite in Xiarihamu deposit, East Kunlun Orrogenic Belt, Qinghai. *Northwest. Geol.* 47, 96–106 [in Chinese with English Abstract]. doi:10.3969/j.issn.1009-6248.2014.01.007

Cao, Z. H., Luo, X. R., and Wang, P. P. (2010). Geoelectro–chemical extraction method for prospecting nickel – cobalt deposit in south Jinchua. *J. Guilin Univ. Technol.* 30, 47–51 [in Chinese with English Abstract]. doi:10.3969/j.issn.1674-9057.2010.01.007

Craig, J. R. (1971). Violarite stability relations. *Am. Mineral.* 56, 1303–1311.

Crocket, J. H., and Fleet, M. E. (1997). Implications of composition for experimental partitioning of platinum-group elements and gold between sulfide liquid and basalt melt: the significance of nickel content. *Geochem. Cosmochim. Acta* 61, 4139–4149. doi:10.1016/s0016-7037(97)00234-2

Du, W. (2018). *Study on two kinds of mafic ultramafic rocks and nickel sulfide deposit in East Kunlun island arc zone*. Xi'an, China: Chang' an University [in Chinese with English Abstract].

Du, W., Ling, J. L., Zhou, W., Wang, Z. X., Xia, Z. D., Xia, M. Z., et al. (2014). Geological characteristics and genesis of Xiarihamu nickel deposit in East Kunlun. *Miner. Depos.* 33, 713–726 [in Chinese with English Abstract]. doi:10.3969/j.issn.0258-7106.2014.04.004

Feng, C. Y., Zhao, Y. M., Li, D. X., Liu, J. N., and Liu, C. Z. (2016). Mineralogical characteristics of the Xiarihamu nickel deposit in the Qiman Tagh mountain, East Kunlun, China. *Geol. Rev.* 62, 215–228 [in Chinese with English Abstract]. doi:10.16509/j.georeview.2016.01.017

Fleet, M. E. (1973). The crystal structure of maucherite ($Ni_{11}As_8$). *Am. Mineral.* 58, 203–210.

Hazen, R. M., Hystad, G., Golden, J. J., Hummer, D. R., Liu, C., Downs, R. T., et al. (2017). Cobalt mineral ecology. *Am. Mineral.* 102, 108–116. doi:10.2138/am-2017-5798

Helmy, H. M., Ballhaus, C., Berndt, J., Bockrath, C., and Wohlgemuth-Ueberwasser, C. (2007). Formation of Pt, Pd and Ni tellurides: experiments in sulfide-telluride systems. *Contrib. Mineral. Petrol.* 153, 577–591. doi:10.1007/s00410-006-0163-7

Helmy, H. M., Ballhaus, C., Fonseca, R. O. C., and Nagel, T. J. (2013). Fractionation of platinum, palladium, nickel, and copper in sulfide-arsenide systems at magmatic temperature. *Contrib. Mineral. Petrol.* 166, 1725–1737. doi:10.1007/s00410-013-0951-9

Helmy, H. M., Ballhaus, C., Wohlgemuth-Ueberwasser, C., Fonseca, R. O. C., and Laurenz, V. (2010). Partitioning of Se, As, Sb, Te and Bi between monosulfide solid solution and sulfide melt - application to magmatic sulfide deposits. *Geochem. Cosmochim. Acta* 74, 6174–6179. doi:10.1016/j.gca.2010.08.009

Huang, W. T., Wu, J., Liang, H. Y., Chen, X. L., Zhang, J., and Ren, L. (2020). Geology, geochemistry and genesis of the Longhua low-temperature hydrothermal Ni-Co arsenide deposit in sedimentary rocks, Guangxi, South China. *Ore Geol. Rev.* 120, 103393. doi:10.1016/j.oregeorev.2020.103393

Jiang, C. Y., Ling, J. L., Zhou, W., Du, W., Wang, Z. X., Fan, Y. Z., et al. (2015). Petrogenesis of the Xiarihamu Ni-bearing layered mafic-ultramafic intrusion, East Kunlun: implications for its extensional island arc environment. *Acta Petrol. Sin.* 31, 1117–1136 [in Chinese with English Abstract]. doi:CNKI:SUN:YSXB.0.2015-04-019

Klemm, D. D. (1965). Synthesen and analysen in den Dreiecks-diagrammen FeAsS–CoAsS–NiAsS und FeS_2–CoS_2–NiS_2. *Neues Jahrbuch Mineral. Abhand.* 103, 205–255.

Li, C., Zhang, Z., Li, W., Wang, Y., Sun, T., and Ripley, E. M. (2015). Geochronology, petrology and Hf-S isotope geochemistry of the newly-discovered Xiarihamu magmatic Ni-Cu sulfide deposit in the Qinghai-Tibet plateau, western China. *Lithos* 216–217, 224–240. doi:10.1016/j.lithos.2015.01.003

Li, W. Y. (2018). The primary discussion on the relationship between Paleo- asian ocean and Paleo-Tethys ocean. *Acta Petrol. Sin.* 34, 3–12 [in Chinese with English Abstract]. doi:CNKI:SUN:YSXB.0.2018-08-001

Li, W. Y., Wang, Y. L., Qian, B., Liu, Y. G., and Han, Y. X. (2020). The discussion on the formation of the magmatic Cu-Ni-Co sulfide deposits in the margin of the Tarim Block. *Earth Sci. Front.* 27, 276–293. [in Chinese with English Abstract]. doi:10.13745/j.esf.sf.2020.3.22

Li, Y., and Audétat, A. (2012). Partitioning of V, Mn, Co, Ni, Cu, Zn, As, Mo, Ag, Sn, Sb, W, Au, Pb, and Bi between sulfide phases and hydrous basanite melt at upper mantle conditions. *Earth Planet Sci. Lett.* 355–356, 327–340. doi:10.1016/j.epsl.2012.08.008

Liang, Q.-L., Song, X.-Y., Wirth, R., Chen, L.-M., and Dai, Z.-H. (2019). Implications of nano- and micrometer-size platinum-group element minerals in base metal sulfides of the Yangliuping Ni-Cu-PGE sulfide deposit, SW China. *Chem. Geol.* 517, 7–21. doi:10.1016/j.chemgeo.2019.04.015

Liu, Y., and Brenan, J. (2015). Partitioning of platinum-group elements (PGE) and chalcogens (Se, Te, As, Sb, Bi) between monosulfide-solid solution (MSS), intermediate solid solution (ISS) and sulfide liquid at controlled fO2-fS2 conditions. *Geochem. Cosmochim. Acta* 159, 139–161. doi:10.1016/j.gca.2015.03.021

Liu, Y., Li, W., Jia, Q., Zhang, Z., Wang, Z., Zhang, Z., et al. (2018). The dynamic sulfide saturation process and a possible slab break-off model for the giant Xiarihamu magmatic nickel ore deposit in the East Kunlun orogenic belt, northern Qinghai-Tibet plateau, China. *Econ. Geol.* 113, 1383–1417. doi:10.5382/econgeo.2018.4596

Lü, L. S., Liu, J., Zhang, Z. H., and Xie, G. Q. (2007). Temporal-spatial distribution and geodymanic settings of magmatic Ni-Cu-(PGE) sulfide deposits in China. *Acta Petrol. Sin.* 23 (10), 2561–2594. doi:10.3969/j.issn.1000-0569.2007.10.024

Lu, S., Li, H., Zhang, C., and Niu, G. (2008). Geological and geochronological evidence for the Precambrian evolution of the Tarim Craton and surrounding continental fragments. *Precambrian Res.* 160, 94–107. doi:10.1016/j.precamres.2007.04.025

Luo, H. B. (1994). Mineralogical Study on the genesis of violarite in magmatic copper nickel deposits. *Geol. Prospect.* 1, 38–40 [in Chinese]. doi:CNKI:SUN:DZKT.0.1994-01-008

Mansur, E. T., Barnes, S.-J., and Duran, C. J. (2019). Textural and compositional evidence for the formation of pentlandite via peritectic reaction: implications for the distribution of highly siderophile elements. *Geology* 47, 351–354. doi:10.1130/g45779.1

Manuel, J., Subías, I., Fanlo, I., Arranz, E., and Gervilla, F. (2018). Multi-isotope survey on the metallogenesis of the hydrothermal Co-Ni deposits in the Alpine

Central Pyrenees of Spain. *Ore Geol. Rev.* 94, 225–238. doi:10.1016/j.oregeorev.2018.01.030

Michener, C., and Peacock, M. (1943). Parkerite ($Ni_3Bi_2S_2$) from Sudbury, Ontario: redefinition of the species. *Am. Mineral.* 28, 343–355.

Moroni, M., Caruso, S., Barnes, S. J., and Fiorentini, M. L. (2017). Primary stratigraphic controls on ore mineral assemblages in the Wannaway komatiite-hosted nickel-sulfide deposit, Kambalda camp, Western Australia. *Ore Geol. Rev.* 90, 634. doi:10.1016/j.oregeorev.2017.05.031

No. 5 Geological and Mineral Survey Institute of Qinghai Province (GMSQH). (2014). Investigation report on HS26 abnormal zone in the Xiarihamu Co-Ni mining area in Golmud City, Qinghai Province, 1–189 (in Chinese).

Piña, R., Gervilla, F., Barnes, S.-J., Ortega, L., and Lunar, R. (2014). Liquid immiscibility between arsenide and sulfide melts: evidence from a LA-ICP-MS study in magmatic deposits at Serranía de Ronda (Spain). *Miner. Depos.* 50, 265–279. doi:10.1007/s00126-014-0534-3

Ponomarenko, A., Kovalenker, V., and Troneva, N. (1987). Parkerite. *Tr. Mineral. Muzeya Akad.* Nauk SSSR 34, 108–114.

Qian, Y., Li, H. R., Sun, F. Y., Sun, J. L., and Wang, G. (2020). Zircon U-Pb dating and sulfide Re-Os isotopes of the Xiarihamu Cu-Ni sulfide deposit in Qinghai province, NW China. *Can. J. Earth Sci.* 57, 8. doi:10.1139/cjes-2019-0107

Raič, S., and Mogessie, A. (2015). Arsenic-enriched Cu-Ni-PGE mineralization in Wetlegs, Duluth complex, St. Louis county, Minnesota, USA. *Can. Mineral.* 53, 105–132. doi:10.3749/canmin.1400053

Roseboom, E. H., Jr. (1962). Skutterudites (Co, Ni, Fe) As3−x: composition and cell dimensions. *Am. Mineral.* 47, 310–327.

Shvedov, G., and Barkov, A. (2017). Primary and alteration assemblages of platinum-group minerals from the Ognit complex, Irkutskaya oblast, Eastern Sayans, Russia. *N. Jb. Miner. Abh.* 194, 35–48. doi:10.1127/njma/2016/0038

Singleton, M., and Nash, P. (1987). The As–Ni (arsenic–nickel) system. *J. Phase Equil.* 8, 419–422. doi:10.1007/bf02893150

Song, X.-Y., Wang, K.-Y., Barnes, S. J., Yi, J.-N., Chen, L.-M., and Schoneveld, L. E. (2020). Petrogenetic insights from chromite in ultramafic cumulates of the Xiarihamu intrusion, northern Tibet Plateau, China. *Am. Mineral.* 105, 479–497. doi:10.2138/am-2020-7222

Song, X.-Y., Yi, J.-N., Chen, L.-M., She, Y.-W., Liu, C.-Z., Dang, X.-Y., et al. (2016). The Giant Xiarihamu Ni-Co sulfide deposit in the East Kunlun orogenic belt, northern Tibet plateau, China. *Econ. Geol.* 111, 29–55. doi:10.2113/econgeo.111.1.29

Spiridonov, E. M., Gritsenko, Y. D., and Ponomarenko, A. I. (2008). Metamorphic-hydrothermal parkerite and associated minerals in the Noril'sk ore field. *Geol. Ore Depos.* 50, 755–762. doi:10.1134/s1075701508080126

Springer, G. (1989). Chlorine-bearing and other uncommon minerals in the strathcona deep copper zone, Sudbury district, Ontario. *Can. Mineral.* 27, 311–313. doi:10.1007/BF01164492

Stefan, K., Axel, G., Benjamin, F. W., Udo, N., Thomas, W., and Gregor, M. (2018). Reconstruction of a >200 Ma multi-stage "five element" Bi-Co-Ni-Fe-As-S system in the Penninic Alps, Switzerland. *Ore Geol. Rev.* 95, 746–788. doi:10.15496/publikation-24256

Tang, Q. Y., Li, J. P., Zhang, M. J., Song, Z., Dang, Y. X., and Du, L. (2017). The volatile conditions of ore-forming magma for the Xiarihamu Ni-Cu sulfide deposit in East Kunlun orogenic belt , western China: constraints from chemical and carbon isotopic compositions of volatiles. *Acta Petrol. Sin.* 33, 104–114 [in Chinese with English Abstract]. doi:CNKI:SUN:YSXB.0.2017-01-009

Tang, Z. L., and Li, W. Y. (1995). *Metallogenic model and geological comparison of Jinchuan Cu-Ni-(Pt-bearing) sulfide deposit*. Beijing: Geological Publishing House, 43–51.

Tenailleau, C., Pring, A., Etschmann, B., Brugger, J., Grguric, B., and Putnis, A. (2006). Transformation of pentlandite to violarite under mild hydrothermal conditions. *Am. Mineral.* 91, 706–709. doi:10.2138/am.2006.2131

Wang, G. (2014). *Metallogenesis of nickel deposits in eastern Kunlun orogenic belt, Qinghai Province*. Changchun, China: Jilin University [in Chinese with English Abstract].

Wang, G., Sun, F. Y., Li, B. L., Li, S. J., Zhao, J. W., Ao, C., et al. (2014a). Petrography, zircon U-Pb geochronology and geochemistry of the mafic-ultramafic intrusion in Xiarihamu Cu-Ni deposit from East Kunlum,with implications for geodynamic setting. *Earth Sci. Front.* 21, 381–401 [in Chinese with English Abstract]. doi:10.13745/j.esf.2014.06.036

Wang, G., Sun, F. Y., Li, B. L., Li, S. J., Zhao, J. W., Yang, Q. A., et al. (2013). Zircon U-Pb geochronology and geochemistry of the early devonian syenogranite in the Xiarihamu ore district from East Kunlun, with implications for the geodynamic setting. *Geotect. Metal.* 37, 685–697 [in Chinese with English Abstract]. doi:10.16539/j.ddgzyckx.2013.04.015

Wang, G., Sun, F. Y., Li, B. L., Li, S. J., Zhao, J. W., and Yang, Q. A. (2014b). Zircon U-Pb geochronology and geochemistry of diorite in Xiarihamu ore district from East Kunlun and its geological significance. *J. Jilin Univ. (Earth Sci. Ed.)* 44, 876–891 [in Chinese with English Abstract]. doi:10.13278/j.cnki. jjuese.201403113

Wang, X. D., Zhang, M. J., Fu, J. R., Zhang, J. W., Li, L. W., Tang, Q. Y., et al. (2018). The magmatic intrusive direction constrains from noble gas isotopic compositions: a case study of the Xiarihamu Ni- Cu sulfide deposit in East Kunlun orogenic belt, China. *Acta Petrol. Sin.* 34, 3433–3444 [in Chinese with English Abstract]. doi:CNKI:SUN:YSXB.0.2018-11-022

Xia, F., Brugger, J., Chen, G., Ngothai, Y., O'Neill, B., Putnis, A., et al. (2009). Mechanism and kinetics of pseudomorphic mineral replacement reactions: a case study of the replacement of pentlandite by violarite. *Geochem. Cosmochim. Acta* 73, 1945–1969. doi:10.1016/j.gca.2009.01.007

Yi, J. N., Song, X. Y., Chen, L. M., and She, Y. W. (2015). Geological characteristics of Xiarihamu superlarge Cu-Ni-Co sulfide deposit in East Kunlun orogen. *Acta Mineral. Sin.* S1, 450, 2015 [in Chinese].

Yund, R. A. (1961). Phase relations in the system Ni-As. *Econ. Geol.* 56, 1273–1296. doi:10.2113/gsecongeo.56.7.1273

Zhang, Z. B., Li, W. Y., Zhang, Z. W., Liu, Y. G., Qian, B., Wang, Y. L., et al. (2016). Characteristics of chromian spinels from the Xiarihamu magmatic Ni-Cu sulfide ore deposit in the eastern Kunlun Orogenic Belt, northwest China and their implication. *Bull. China Soc. Mineral Petrol. Geochem.* 35, 966–975 [in Chinese with English Abstract]. doi:10.3969/j.issn.1007-2802.2016.05.017

Zhang, Z. W., Qian, B., Wang, Y. L., Li, S. J., and Liu, C. Z. (2016). Petrogeochemical characteristics of the Xiarihamu magmatic Ni-Cu sulfide deposit in Qinghai province and its study for olivine. *Northwest Geol.* 49, 45–58 [in Chinese with English Abstract]. doi:10.3969/j.issn.1009-6248.2016.02.005

Zhao, J., Li, G., Qin, K., and Tang, D. (2019). A review of the types and ore mechanism of the cobalt deposits. *Chin. Sci. Bull.* 64, 2484–2500 [in Chinese]. doi:10.1360/n972019-00134

Conflict of Interest: The authors declare that the research was conducted in the absence of any commercial or financial relationships that could be construed as a potential conflict of interest.